

Traveling waves in quasi one-dimensional neuronal minicolumns

Vincent Baker, vjb42@drexel.edu¹

Luis Cruz, ccruz@drexel.edu¹

¹Drexel University, Department of Physics.

Keywords: Traveling waves, one-dimensional networks, minicolumns, microcolumns, cortical organization, time delay, balanced excitation and inhibition

Abstract

Traveling waves of neuronal activity in the cortex have been observed *in vivo*. These traveling waves have been correlated to various features of observed cortical dynamics including spike timing variability and correlated fluctuations in neuron membrane potential. Although traveling waves are typically studied as either strictly one-dimensional or two-dimensional excitations, here we investigate the conditions for the existence of quasi one-dimensional traveling waves that could be sustainable in parts of the brain

containing cortical minicolumns. For that, we explore a quasi one-dimensional network of heterogeneous neurons with a biologically influenced computational model of neuron dynamics and connectivity. We find that background stimulus reliably evokes traveling waves in networks with local connectivity between neurons. We also observe traveling waves in fully-connected networks when a model for action potential propagation speed is incorporated. The biological properties of the neurons influence the generation and propagation of the traveling waves. Our quasi one-dimensional model is not only useful for studying the basic properties of traveling waves in neuronal networks, but it also provides a simplified representation of possible wave propagation in columnar or minicolumnar networks found in the cortex.

1 Introduction

Connected neurons that fire sequentially can stimulate firings from neighboring neurons, creating a traveling wave of neuron spikes. These traveling waves have been observed in the cortex of mammalian brains (Muller, Chavane, Reynolds, & Sejnowski, 2018)(Reimer, Hubka, Engel, & Kral, 2011) as well as in vitro (Wu, Huang, & Zhang, 2008)(Huang et al., 2004)(Golomb & Ermentrout, 1999), and subsequently have been reproduced in silico (Keane & Gong, 2015)(Senk et al., 2020)(Golomb, Wang, & Rinzel, 1996)(G. Bard Ermentrout & Kleinfeld, 2001). While the function of traveling waves is unknown (Wu et al., 2008)(Muller et al., 2018), proposed functions include motor coordination (Rubino, Robbins, & Hatsopoulos, 2006) , place field coordination in the hippocampus (Lubenov & Siapas, 2009), and spatiotemporal processing in the visual

cortex (Wu et al., 2008)(Muller, Reynaud, Chavane, & Destexhe, 2014).

Neuronal traveling waves are not uniquely defined as they can exist at widely differing frequency and scale lengths. In the sleep and anesthetized states, slow and large-scale wave activity has been recorded (Muller et al., 2018). Traveling waves have been detected in local-field potentials measured with electrodes (Rubino et al., 2006)(Sanes & Donoghue, 1993)(Riehle, Wirssohn, Grün, & Brochier, 2013). Local-area traveling waves in the awake cortex have been observed using recent advances in optical imaging techniques using voltage-sensitive dyes (Wu et al., 2008)(Shoham et al., 1999)(Xu, Huang, Takagaki, & young Wu, 2007)(Ferezou, Bolea, & Petersen, 2006). Similarly, traveling waves also differ by the manner in which they are created. Both spontaneously occurring waves and stimulus-evoked (Reimer et al., 2011) waves have been observed in the visual and auditory cortex. Computational and mathematical modeling of traveling waves in a variety of models have shown many of the characteristics observed experimentally (G. Bard Ermentrout & Kleinfeld, 2001)(Keane & Gong, 2015)(Gibson, Belerlein, & Connors, 1999).

Studies of traveling waves have focused on two-dimensional waves that spread parallel to the surface (pia) of the brain (Reimer et al., 2011)(Keane & Gong, 2015)(Townsend & Gong, 2018)(Golomb & Amitai, 1997)(Qi & Gong, 2015). This is to be expected as this is the geometry of the system on which they are observed, and (Wilson & Cowan, 1973) provide an anatomical argument for focusing on such structure. Traveling waves in one-dimensional neuronal systems have been previously explored using several theoretical methods. In the literature on neural fields (G. B. Ermentrout & Cowan, 1979)(Folias & Ermentrout, 2012) and coupled oscillators (Kopell & Ermen-

trout, 1986)(Williams & Bowtell, 1997) isotropic networks of homogeneous neurons with symmetric synaptic coupling give rise to field models which exhibit traveling wave solutions for certain parameter values. One-dimensional waves have also been observed in simulations using firing rate neurons (Roxin, Brunel, & Hansel, 2005), integrate-and-fire neurons (Bressloff & Coombes, 1997)(Golomb & Ermentrout, 1999) and Hodgkin-Huxley neurons (Golomb & Amitai, 1997). (Senk et al., 2020) used populations of both rate neurons and integrate-and-fire neurons and developed a method to translate parameters between the two different models.

These simulations again use homogeneous neuronal populations in networks that are invariant to spatial translation, resulting naturally in periodic spatio-temporal patterns. These purely one-dimensional systems may not be robust to realistic variation in neuron properties, connectivity and noise. This is exemplified in (Senk et al., 2020) where traveling waves are only observed for certain parameter values, and (Strogatz & Mirollo, 1991) where the stability of systems of coupled oscillators can be radically altered by including infinitesimal noise. Our current work explores traveling waves in quasi-one-dimensional networks with substantial randomness in both individual neurons (randomly selecting type and randomizing dynamical parameters), connectivity between neurons, and stimulus to the neurons.

Previous studies have used one-dimensional structures largely for their computational or analytic simplicity. Consideration of a quasi one-dimensional system may seem as an unnecessary complication, but there is no a priori reason that quasi one-dimensional traveling waves may not be found *in vivo*. Of interest, there are regions of the brain where there are what seem to be quasi one-dimensional structures (Buxho-

eveden & Casanova, 2002)(Mountcastle, 1997) typically called micro- or minicolumns. These minicolumns are aligned perpendicular to the pia and can be hundreds of microns long. Although their relevance to cognition and function is still being debated (Horton & Adams, 2005)(Cruz et al., 2009)(Buxhoeveden & Casanova, 2002), it is possible that they can sustain traveling waves.

To address this possibility, here we investigate the conditions under which traveling waves can exist on quasi one-dimensional systems, and their fundamental properties and dynamics. Inspired by minicolumns, our systems consist of thin (few neuron) and long (~ 100 neuron) networks of locally connected neurons placed on a three-dimensional lattice. We model the neuron dynamics using the Izhikevich model (Izhikevich, 2003) that allow us to explore more complex neuron dynamics than typically afforded by integrate-and-fire models (Keane & Gong, 2015)(Senk et al., 2020) while also providing a distribution of neuron dynamical parameters that mimics the type and variety of neurons observed in the mammalian cortex. We use a morphology and connectivity model inspired by (Maass, Natschläger, & Markram, 2002), incorporating a local connectivity model (Levy & Reyes, 2012)(Pyle & Rosenbaum, 2017)(Fino & Yuste, 2011). To incorporate elements of a real brain, we consider a model with substantial randomness in both individual neurons and connections between neurons while also considering distance-dependent time delays in the propagation of action potentials.

Among our main findings we determine parameters in our model that allow for the generation of traveling waves in our quasi one-dimensional systems. These traveling waves exhibit properties such as spontaneous creation from a random background stimulus, annihilation of colliding waves, and a wave velocity that is determined by both the

propagation speed of the action potential and the neuron dynamics. Traveling waves are present in both locally-connected and fully-connected systems. The traveling waves in fully connected systems are dependent upon the action potential propagation speed, while traveling waves can propagate in locally-connected systems even when action potential propagation is instantaneous.

2 Methods

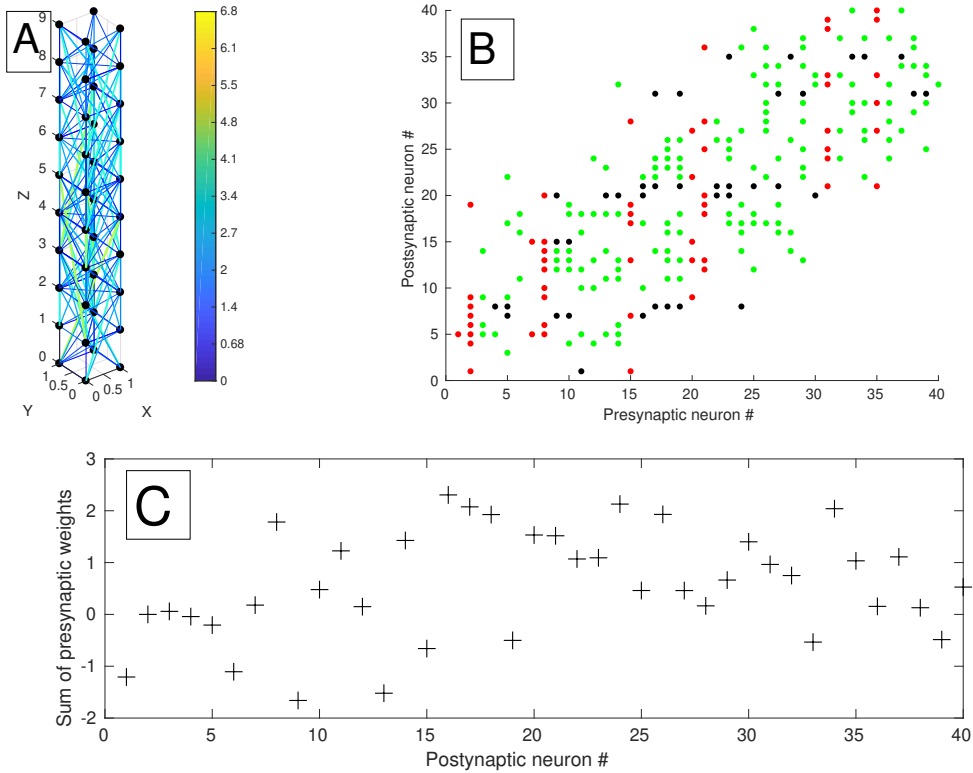
To study traveling waves in small columnar ensembles (SCE) of neurons we created a MATLAB simulation of our model based on (Izhikevich, 2003) . We first construct these assemblies by placing neurons at the vertices of a cubic lattice described by two short dimensions (X,Y) and one long dimension (Z). Each neuron is randomly chosen to be either excitatory (E) or inhibitory (I), with the fraction of excitatory neurons indicated as P_{exc} . After placing, we connect two neurons based on their relative distance according to a connection probability that favors local connectivity given by (Maass et al., 2002):

$$P_{a,b} = C e^{-(D(a,b)/\lambda)^2} \quad (1)$$

where $D(a, b)$ is the Euclidean distance between neuron A and B, λ is the characteristic length of the local connectivity neighborhood, and C is the peak probability of connection . In (Levy & Reyes, 2012) the authors showed that the synaptic connections in the mouse auditory cortex follow this connection probability. Multiple connections from the same presynaptic neuron to the same postsynaptic neuron, as well as self-connections, are prohibited. Two neurons may be recurrently connected, however. An

example of an SCE showing the connectivity structure is shown in Figure 1. We use

Figure 1: Example SCE with dimensions 2x2x10 (XxYxZ), $\lambda=2.5$, and $C=1$. A) SCE showing connections between neurons as lines colored using a color scale that indicates the connection length. B) Connection matrix. E-E connections are green, E-I are black and both I-E and I-I are red. The labels of the neurons used in both axes are sequentially assigned starting at the bottom ($Z=0$). C) The sum of presynaptic weights for each neuron shows the anisotropy of this model, with substantial variation in input strength and sign between the neuron inputs.



open boundary conditions, so neurons near the ends of the SCE will have fewer connections than those in the middle.

We model the firing dynamics of each neuron using the Izhikevich model (Izhikevich, 2003) that consists of a two-dimensional model of two coupled differential equa-

tions given by:

$$\begin{aligned} v' &= 0.04v^2 + 5v + 140 - u + I \\ u' &= a(bv - u) \end{aligned} \tag{2}$$

where v is the membrane potential of the neuron and u is a membrane recovery variable, with a spike threshold and an auxilliary after-spike resetting of parameters by:

$$\text{if } v > 30 : v \leftarrow c, u \leftarrow u + d \tag{3}$$

and I is the sum of all incoming currents to the neuron, explained in detail below.

Equation 2 has four parameters (a,b,c,d) that with specific values can model a wide range of neuronal spiking behavior (Izhikevich, 2003). The parameters used here (see Table 1) are based on those specified in (Izhikevich, 2003) with modification of the c parameter for excitatory neurons and define a random population of neurons where $U(s, t)$ represent a number drawn from a uniform random distribution between s and t. For solving equation (2) numerically we use the modified Euler method from (Izhike-

Table 1: Izhikevich model parameters

Parameter	Excitatory	Inhibitory
a	0.02	$0.02 + \mathcal{U}(0, 0.08)$
b	0.2	$0.25 - \mathcal{U}(0, 0.05)$
c	$-65 + \mathcal{U}(0, 10)^2$	-65
d	$8 - \mathcal{U}(0, 6)$	2

vich, 2003) with a time step of $0.2ms$ except were noted.

A crucial element to evoke traveling waves in neuronal systems is the existence of time delays between the creation of a presynaptic action potential and the arrival of

that spike to a target neuron. For this, we use distance-dependent time delays for the propagation of a spike from neuron i to neuron j of $\tau_{ij} = \kappa D(i, j)$. The constant of proportionality κ ranges from 0 to 4. When $\kappa = 0$ the action potential excites the post-synaptic neuron on the succeeding simulation time step.

The current I in equation (2) includes the sum of all incoming stimuli into neuron i from other neurons I_i and external stimuli $I_{i,e}$ applied to the system. The neuron-neuron incoming current I_i into neuron i is given by:

$$I_i(t) = \sum_{j \neq i} \sum_{t'_j} S_{ij} \Theta(t - t'_j - \tau_{ij}) e^{-(\frac{t - t'_j - \tau_{ij}}{\sigma_s})^2} \quad (4)$$

where t'_j are the firing times of neuron j , Θ is the Heaviside step function, and the exponential factor models an exponentially decaying synapse response with a time constant of $\sigma_s = 4ms$. The S_{ij} represent the connection strengths between presynaptic neuron j and postsynaptic neuron i given by

$$\begin{aligned} S_{ij}^{excitatory} &= K \times \mathcal{U}\{0, 0.5\} \\ S_{ij}^{inhibitory} &= K \times \mathcal{U}\{-1, 0\} \end{aligned} \quad (5)$$

where K is a parameter that modulates the strength of connections, with $K = 1$ corresponding to the original model in (Izhikevich, 2003).

To drive the firing dynamics and create traveling waves we provide stimulation to the systems by using two different and separate external stimulus currents, $I_{i,e}$. One of them is a uniform background stimulus applied to each neuron k that depends on whether the neuron is excitatory or inhibitory. The stimulus values are drawn from a

random distribution every $1ms$ according to:

$$\begin{aligned} I_k^{excitatory} &= M \times \mathcal{U}\{0, 1\} \\ I_k^{inhibitory} &= \frac{2}{5}M \times \mathcal{U}\{0, 1\} \end{aligned} \quad (6)$$

where M is a parameter that tunes the overall strength of the stimulus, with $M = 5$ corresponding to the original model in (Izhikevich, 2003). This stimulus has the effect of creating waves that originate from any point along an SCE and one of the uses is to study interactions between multiple waves in section 3.3.

The other external stimulus $I_{i,e}$ is a short constant input of current applied to all of the neurons in the lowest ten layers of an SCE. The duration of the stimulus is $20ms$ with a current of strength 5 units. This stimulus has the effect of creating a single wave that can propagate through the total length of an SCE. One of the uses of this stimulus is to measure the speed of the traveling wave in section 3.2.

For every simulation we record all of the spikes from all neurons. We visualize the spikes in spike raster plots (e.g. Figure 3). Because here we focus on traveling waves in the Z direction, we plot the spikes according to the Z position of the neurons. As a consequence, at each Z position there are multiple neurons that could contribute to the spike raster plot at that Z coordinate (e.g. 4 neurons for the $X=2, Y=2$ SCE case).

To automatically identify waves we perform a spatial clustering operation to this data to identify spatiotemporal regions identified by high firing density. The clustering operation produces an output cluster for any group of more than 3 spike events that fall within a $20ms$ time window from neurons that are no more than 3 layers apart. Each cluster $C(t, z)$ has a time t and position z . This clustering removes random background firing activity. The waves are identified using a plane sweep algorithm that proceeds

along the dimension of simulation time and applies wave labels to clusters such that all clusters with the same label are part of the same wave. When a new cluster $C(t, z)$ is encountered, the algorithm associates $C(t, z)$ with any existing wave if the existing wave has a cluster $C(t_c, z_c)$ within 40ms and 6 units of the new cluster. If there is no such adjacent cluster a new wave is created using $C(t, z)$ as the first cluster. An example of the clustering and identification is shown in Figure 2, with further illustration in SI Figure 1.

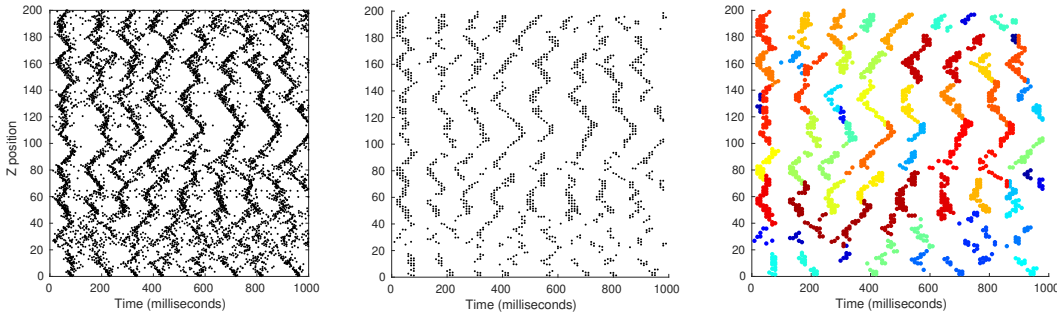


Figure 2: Wave identification and labeling using an example SCE with dimensions $2 \times 2 \times 200$. Left: Raster plot of firing events where dots represent neuronal action potentials. Traveling waves can be seen as diagonal structures of dense firing activity. Center: The clustering operation removes background spikes. Right: Individual waves are labeled with unique identifiers color coded in the figure.

Once identified and labeled, we measure wave propagation speeds and wave initiation locations. We also measure the "wave firing fraction" defined as the fraction of spikes that are associated with the labeled traveling wave (total number of spikes found within the waves divided by number of spikes in the simulation).

Our exploration of the behavior of traveling waves in an SCE involves testing properties of these waves as a function of the different parameters of our model. For

determining existence of traveling waves we use a $2x2x100$ SCE with background stimulation (Eq 6) and vary parameters around a neighborhood of the reference point $\Sigma = \{K = 10, \lambda = 2.5, P_{exc} = 0.8, \kappa = 1.0\}$ that we have determined can sustain traveling waves. To measure wave propagation speed we use a $2x2x50$ SCE with a step stimulus applied to the lowest layers of the SCE and adjust our reference point to be $\Sigma_v = \{K = 24, \lambda = 2.5, P_{exc} = 0.8, \kappa = 1.0\}$. This reference point was selected after inspecting the SCE behavior under a wide range of parameter values. The increase in K is required when using the step stimulus because the higher layers of the SCE do not receive any stimulus. This requires stronger connections so that the traveling wave can elicit spikes from neurons resting at equilibrium.

3 Results

The results are organized as a series of computational experiments on traveling waves. We first determine which parameterizations of our model support traveling waves. Stronger and more numerous local connections between neurons are found to facilitate the formation of traveling wave patters. We then investigate the influence of neuron dynamics and connectivity on the speed of traveling waves. Stronger neuronal connections and faster action potential propagation are shown to increase traveling wave speed, but the neuron dynamics enforce an upper limit on the speed. Low-threshold-spiking inhibitory neurons are shown to consistently generate traveling waves through the mechanism of post-inhibitory rebound spiking. The low-threshold-spiking inhibitory neurons also suppress traveling waves that originate from other points in the SCE. Finally, we exam-

ine fully-connected networks and observe that traveling wave patterns can still emerge provided the action potential propagation speed is slow enough.

3.1 Conditions for the existence of traveling waves in an SCE

We first explore which parameterizations of our model will support traveling waves. We detect the waves as described in Methods, and then use the wave firing fraction metric to determine for which parameter values our model will produce traveling waves. We fix the connection normalization constant C in equation 1 to 0.5 and we fix the stimulus strength M in equation 6 to 5. For this value of C and $\lambda = 2.5$ each neuron has an average of 6.90 input connections, as measured across 100 randomly-generated SCE (see SI Figure 2 for connectivity distribution).

The key parameters of our model that we examine are the connection strength K , the characteristic connection length λ , the fraction of excitatory neurons P_{exc} and the delay parameter κ . First we establish that traveling waves are observed at the reference point $\Sigma = \{K = 10, \lambda = 2.5, P_{exc} = 0.8, \kappa = 1.0\}$. We then vary the individual parameters about Σ to examine how they influence traveling wave formation.

At the reference point Σ the average wave firing fraction over 100 trials is found to be 88.6% with a standard deviation of 4.38%. A representative raster plot of the spike events (Figure 3) clearly shows the traveling waves.

The effect of varying the parameters on traveling waves are shown in Figure 4. The graphs of the wave firing fraction versus K , λ and P_{exc} show similar behavior. Traveling waves are not supported for low values of these parameters. As the parameter values increase traveling waves emerge, and as the parameters grow large the traveling waves

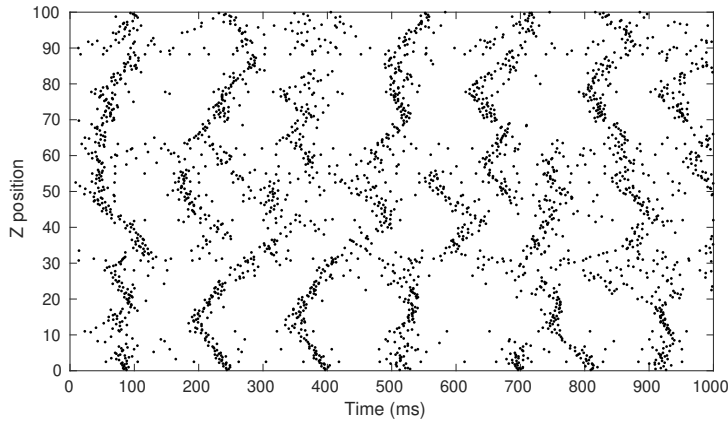


Figure 3: Raster plot of neuron firing events over time. The model parameters are at the reference point Σ . Each dot represents the spike-time emission of a neuron. Traveling waves can be seen as diagonal structures of dense firing activity (Senk et al., 2020).

dominate the firing activity. Stronger connections (K) or more numerous connections (λ) makes it easier for firing activity to spread to adjacent neurons. A higher excitatory fraction acts similarly to a higher connection strength. As the presynaptic activity to each neuron is more excitatory and less inhibitory, it is easier for the traveling wave to propagate. These data suggest that these three parameters all work towards strengthening the local neighborhood of neurons and facilitating the propagation of coordinated spikes as traveling waves.

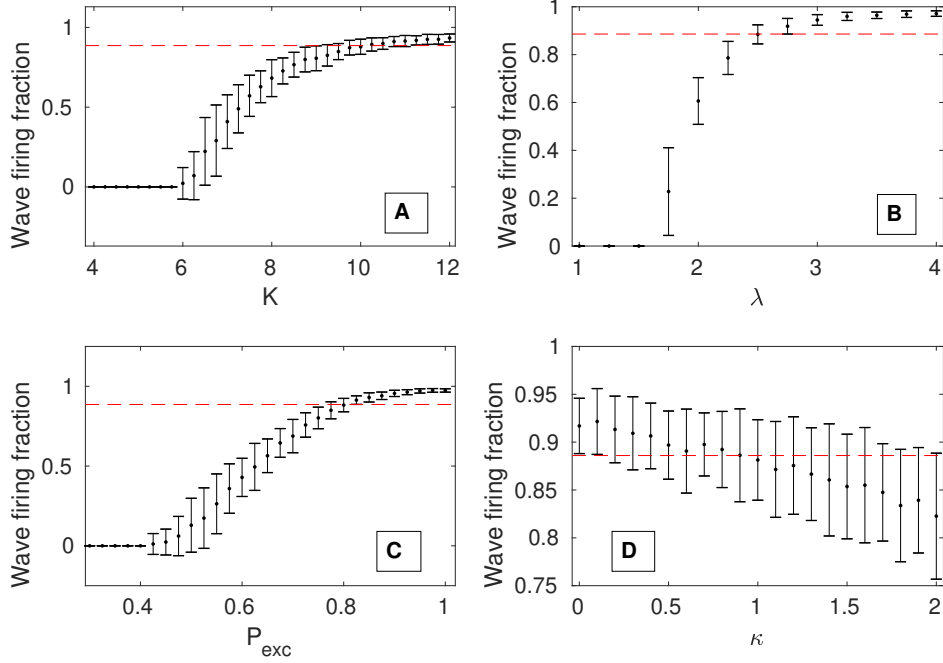


Figure 4: Onset of traveling waves as a function of model parameters in the neighborhood of Σ (100 trials for each parameter value, error bars 1σ). The dashed red lines show the wave firing fraction at the reference point Σ . Varying each individual parameter while holding the other parameters at their Σ values, we observe onset of traveling waves at $K = 6$ (A), $\lambda = 1.5$ (B), and $P_{exc} = 0.45$ (C). D) Traveling waves are present at all values of κ .

For the range of values tested, the parameter κ does not show a strong influence on the existence of traveling waves. This is in contrast to previous work in largely isotropic networks and neural field models which found that the delay parameter is important for the emergence of traveling waves (Senk et al., 2020)(Atay & Hutt, 2006)(Roxin et al., 2005). However, it is consistent with other work that found traveling wave patterns without including propagation delay (Folias & Ermentrout, 2012)(Wyller, Blomquist, & Einevoll, 2007).

A natural question is whether the few long connections along the Z direction that cannot exist in the X or Y directions exert a dominant role on these results. By performing the same experiments as in Figure 4, but now pruning long-range connections, results show that the influence of the longer connections is minimal (SI Figure 4).

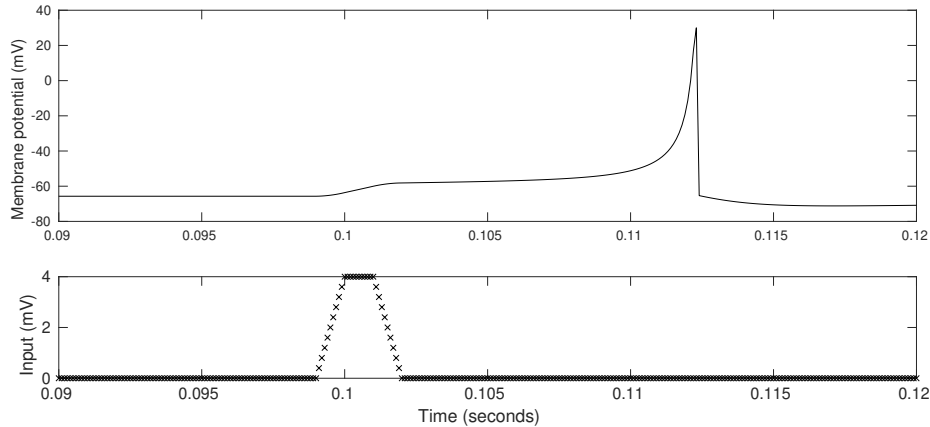
3.2 Wave propagation speed

Cortical traveling waves have been observed with propagating speeds from less than 0.1 to more than 0.8 meters per second (Sato, Nauhaus, & Carandini, 2012)(Golomb & Amitai, 1997)(Chervin, Pierce, & Connors, 1988). This is consistent with the action potential propagation speeds in the gray matter of the cortex (Muller et al., 2018). This suggests that the dynamics of action potential propagation influence wave propagation. To consider the possibility of this relationship we incorporate in our model an action potential propagation time proportional to the distance between the neurons.

Action potential velocity may not be the only factor in the traveling wave propagation speed. In (Golomb & Amitai, 1997) the authors neglected action potential propagation in their model of disinhibited cortical slices as they considered their observed wave velocity of $0.15m/s$ to be an order of magnitude faster than axon potential propagation. In (Chervin et al., 1988) the authors found an even slower propagation of $0.06 - 0.09m/s$ in disinhibited slices of rat cortex. In (Markram, Lübke, Frotscher, Roth, & Sakmann, 1997) a latency of $1.7 \pm 0.9 ms$ was observed between injecting a stimulus in one pyramidal neuron and the resulting excitatory post-synaptic potential in an adjacent pyramidal neuron. This latency is too large to be due solely to axonal propagation alone given the very short distance between the neurons. These results

indicate that a second key element, namely neuron and synapse dynamics, will also influence wave propagation speed. Biological neurons and synapses have complex internal dynamics, and will not fire instantaneously upon receiving a stimulus. The input may push the neuron's dynamical system out of equilibrium and cause a spike, but the system dynamics take some time to evolve. Therefore the spike will occur with some delay after the stimulus. This is a common behavior in any multidimensional model of neuron dynamics, but it is not captured by the leaky integrate-and-fire model used in much of the previous research (Keane & Gong, 2015)(Senk et al., 2020). As an example, Figure 5 shows the delayed response of a neuron to a pulse of current using the Izhikevich model.

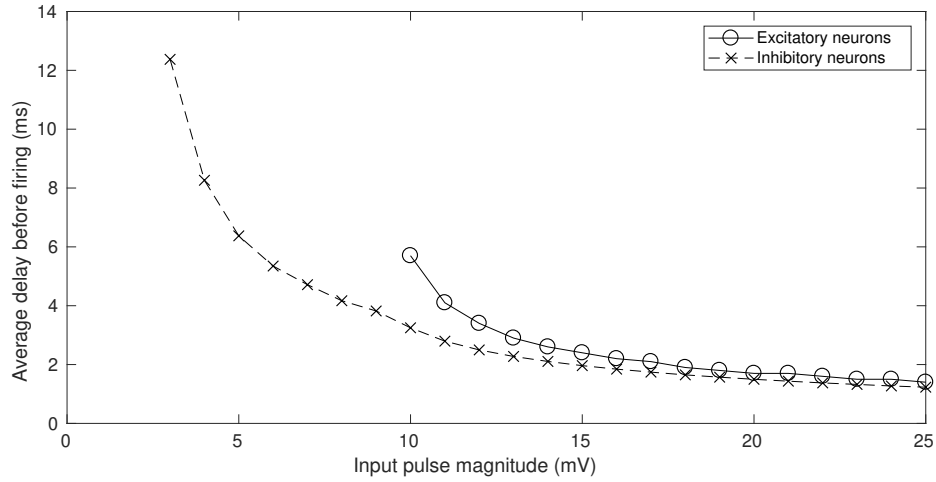
Figure 5: A pulse of voltage (bottom) with magnitude 2mV, starting at t = 100ms and lasting 2ms disturbs the equilibrium membrane potential of a neuron (top), eliciting a spike at t = 112ms.



To determine that this spike delay is indeed important to consider we expose populations of excitatory and inhibitory neurons to current pulses of different magnitudes. The average firing delay of the excitatory and inhibitory neurons is shown in Figure 6. The inhibitory neurons have a lower firing threshold than the excitatory neurons due

to their higher value of b in Equation 2 (Izhikevich, 2003) and fire with a shorter delay when given the same stimulus. Both excitatory and inhibitory neurons exhibit a delayed response of several ms or more.

Figure 6: A stronger stimulus creates a spike with less delay. The excitatory neurons have a higher firing threshold than the inhibitory neurons and do not emit a spike for very weak stimulus.



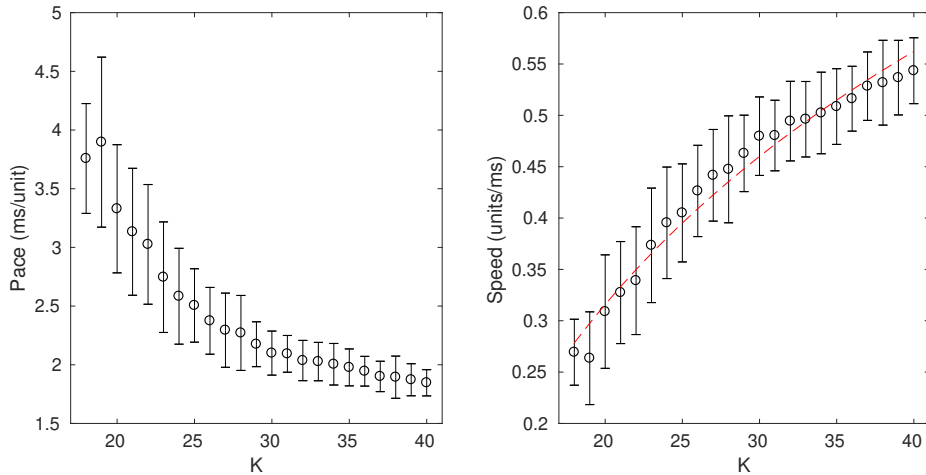
To measure wave propagation speed we use an SCE with width 2, height 2, and length 50. Our exploration of wave speed uses a step stimulus applied to the lowest 10 layers of neurons (see Methods), while no stimulus is applied to the remaining neurons. We then measure the time for the wave to propagate to the top layer to determine the pace in milliseconds per unit length traveled. The speed is then calculated as the inverse of the pace in units/millisecond.

We fix the connection normalization constant C in equation 1 to 0.5 and we fix the stimulus strength M in equation 6 to 5 and do not vary them. As mentioned in Methods we use Σ_v here, with $K = 24$, because the SCE cannot sustain traveling waves at Σ . Here, without the uniform background stimulus the neurons in the SCE are at their

equilibrium point when the traveling wave arrives, and it takes a stronger stimulus from the passing wave to elicit a spike. We increase the connection strength K to provide this stronger stimulus, and find traveling waves that span the SCE starting at $K = 18$. As K increases the neurons fire with less delay, resulting in faster traveling waves (Figure 7). We fix $\Sigma_v = \{K = 24, \lambda = 2.5, P_{exc} = 0.8, \kappa = 1.0\}$ for the remainder of the wave speed computational experiments.

We first examine the impact of K on the wave speed. The wave speed increases with K as anticipated (Figure 7). The relationship is logarithmic in shape, in agreement with some previous work including (Golomb & Ermentrout, 1999) (Figure 3 for $\tau_d > 0$) and (Golomb et al., 1996)(Figure 10, exponential footprint shape).

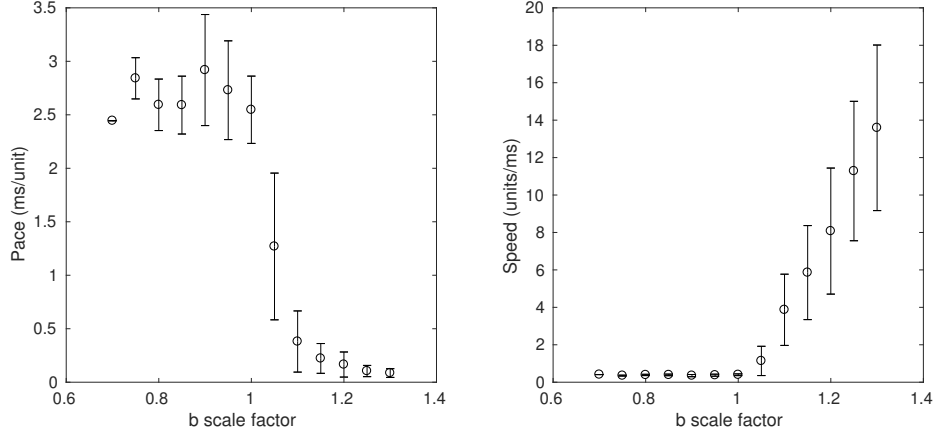
Figure 7: The pace (left, error bars $\pm 1\sigma$) decreases with K , while the corresponding wave speed (right) increases with K . The logarithmic best fit is $0.36 \log 0.12K$.



We examine the influence of the b parameter on wave speed. We generate 100 SCE, then multiply the b parameter of all neurons by a scaling factor from 0.7 to 1.3. When the scale factor is ≤ 1.0 the wave speed remains constant, but when the scale factor is > 1.0 the wave speed increases linearly (Figure 8). This indicates that the lower firing

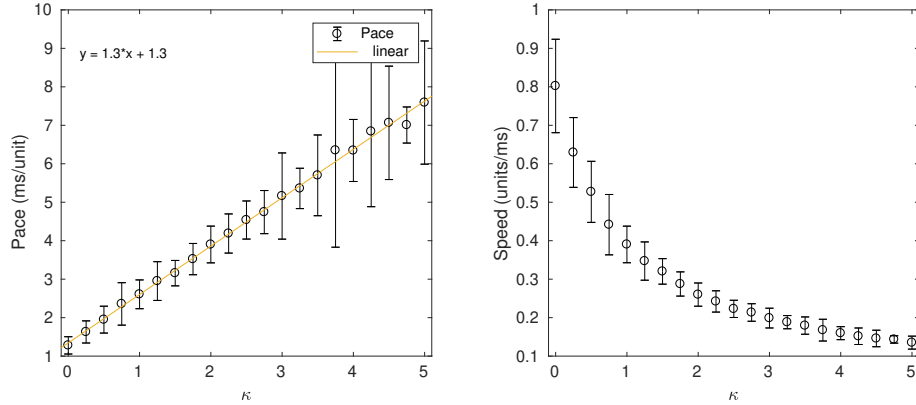
thresholds (Figure 6) that result from larger values of the b parameter result in faster traveling waves.

Figure 8: The pace (left, error bars $\pm 1\sigma$) and the wave speed (right) show a sharp transition above scale factor 1.0.



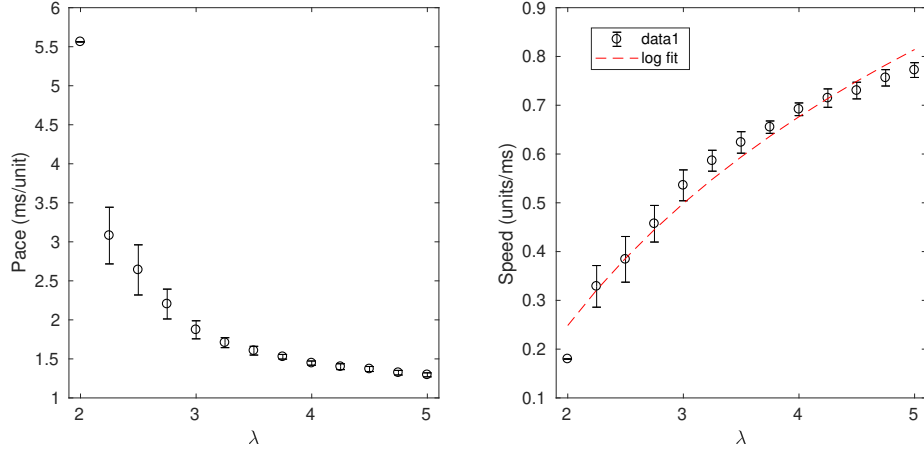
We next explore the influence of the action potential propagation speed, here controlled by our parameter κ , on the traveling wave propagation speed. We vary delay parameter κ from 0 to 5 and measure the wave pace and calculate the wave speed (Figure 9). The pace is linear in κ as expected, but the pace does not approach 0 as $\kappa \rightarrow 0$ due to the delayed firing inherent in the neuron dynamics. Because each neuron does not fire instantaneously upon receiving an action potential, even instantaneous transport of action potentials does not result in a wave that can span the column instantaneously.

Figure 9: The pace (left, error bars $\pm 1\sigma$) is linear w.r.t. κ . The intercept at $\kappa = 0$ is 1.3, indicating that the neuron dynamics limit the speed of the wave. The wave speed (right) shows the expected relationship.



Propagation speed is also influenced by the characteristic length of the local connectivity, λ . Since an increase in λ results in both longer range connections, and more incoming and outgoing connections per neuron, we expect λ to increase the wave speed through both action potential propagation and neuron dynamics. The characteristic connection length λ is varied from 2 to 5 and we measure the wave pace and calculate the wave speed (Figure 10). For $\lambda < 2$ we do not observe traveling waves.

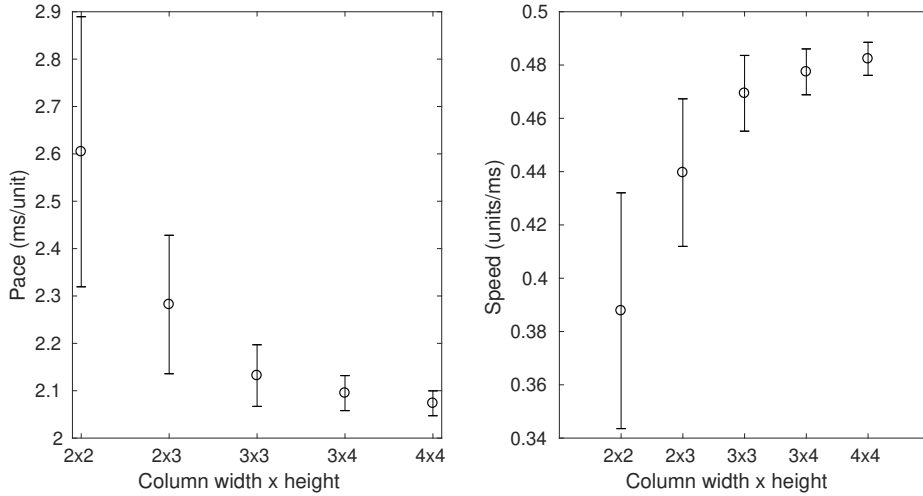
Figure 10: The pace (left, error bars $\pm 1\sigma$) decreases with λ . The wave speed (right) shows that the maximum wave speed approaches 0.8, the limit seen as $\kappa \rightarrow 0$ in Figure 9. The logarithmic best fit to the data is $0.62 \log 0.74\lambda$.



Our SCE topology (namely, the X and Y dimensions) may influence the wave speed in several ways. Increasing X and/or Y increases the total number of neurons, the total number of connections, and the average number of connections per neuron. To test these, we construct columns with topology in XxY of 2x2, 2x3, 3x3, 3x4 and 4x4. We also tested the 1x1 topology but found that it did not support traveling waves (SI Figure 6). For each topology we measure the pace and speed over 5 randomly generated SCE (Figure 11). We see that increasing the X and/or Y dimensions of the SCE increases the speed, and the dependence looks qualitatively similar to increasing the connection strength via K or the number of connections via λ .

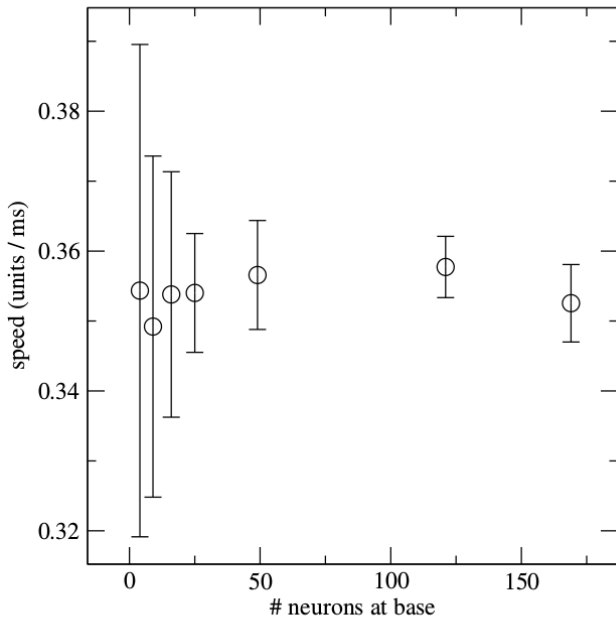
To separate the effect of the increased connectivity from the effect of different topology (larger X or Y increases both the total number of neurons and changes the proportion of surface neurons) we scale the C parameter in equation 1 to maintain the same average number of connections per neuron (~ 7) across the topologies. Results show that

Figure 11: The pace (left, error bars $\pm 1\sigma$) decreases, and the speed (right) increases, as the XxY extents of the SCE grow.



when separated from the increase in connectivity larger cross sections do not change the wave propagation speed (Figure 12). Therefore the increase in speed with cross-section seen in Figure 11 is due entirely to the increasing number of connections per neuron. Figure 5 in the SI shows additional analysis of SCE with larger cross sections.

Figure 12: Wave speed (error bars 1σ) is constant as the topology changes as long as the average number of connections (7 connections per neuron) is maintained. The largest topology is 13×13 (169 neurons at base).

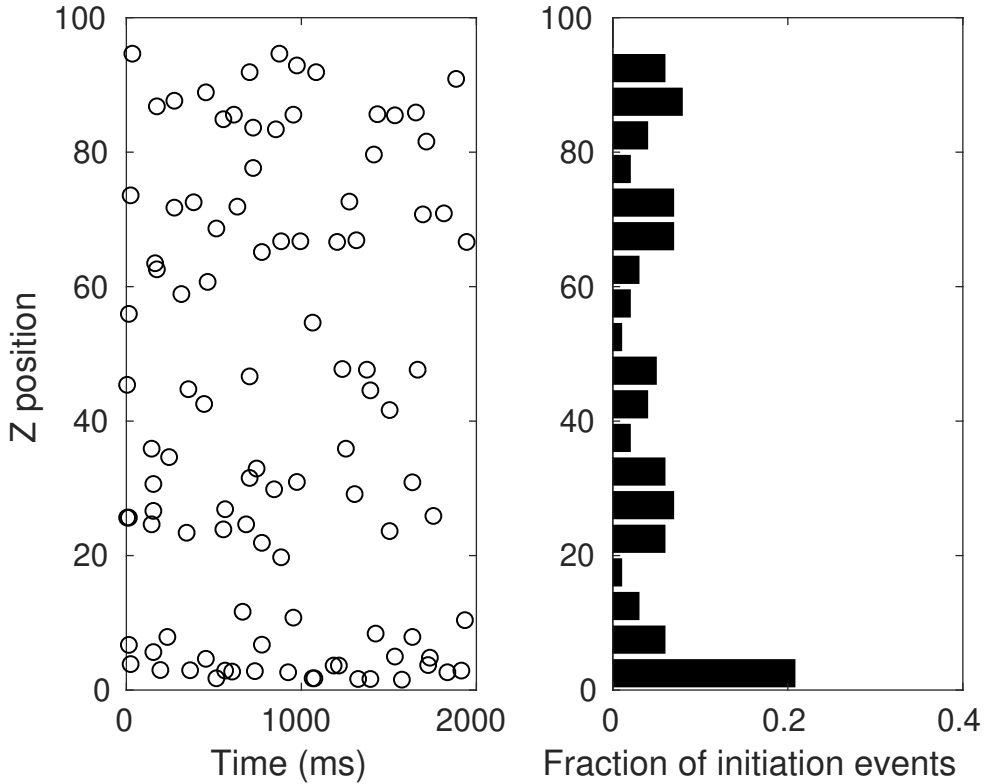


It is interesting to compare the speeds obtained here with previous work. We have placed our neurons on a unit grid and measured speed in units per millisecond. By assuming that our unit grid is about $20 \mu m$ (Cruz et al., 2005) then our wave propagation speeds are in the range of $2 - 16 mm/s$. This is generally slower than other computational results, but the mid to upper range is of the same order of magnitude as the experimental velocity of $50 mm/s$ reported in (Golomb & Amitai, 1997).

3.3 Wave Initiation and Density

Traveling waves spawned by uniform background stimulation do not appear to originate at random places in the SCE. Instead we observe that, for a given randomly generated SCE, waves tend to spawn from certain locations within the SCE. This is most noticeable for SCEs with very dense local connectivity with $C = 1.0$ in equation 1. To quantify this observation we record the initiation sites of all traveling waves that were observed in an SCE under uniform background stimulus (Figure 13). We then measure the fraction of wave initiation events (FIE) per unit length of the SCE.

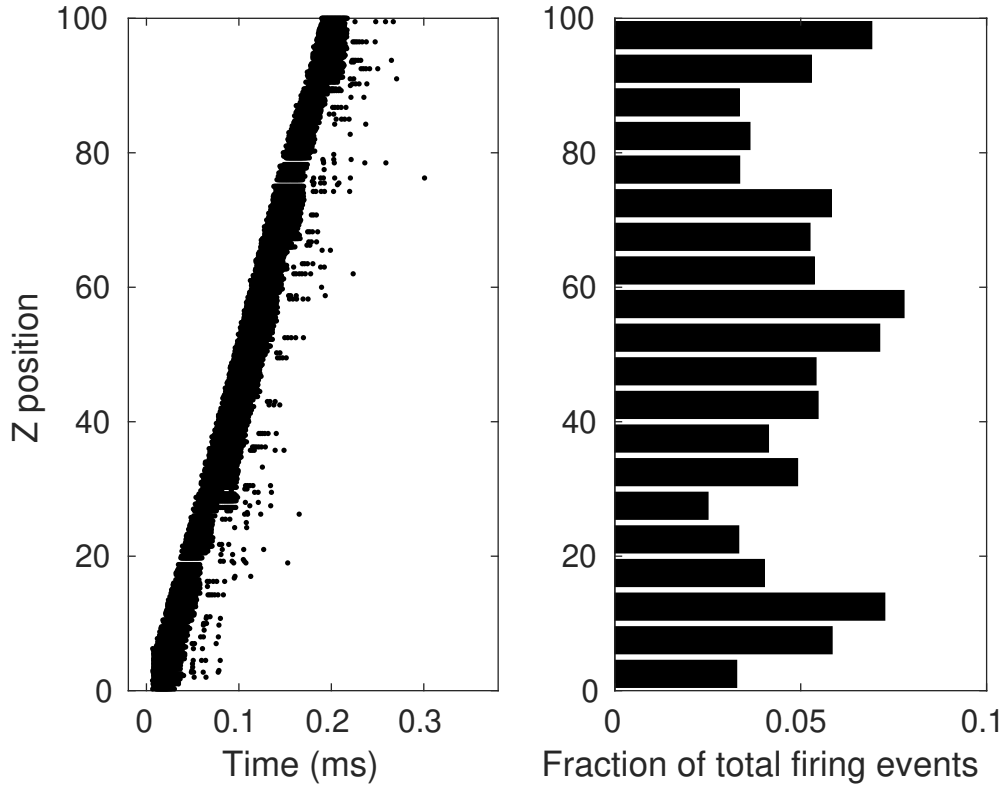
Figure 13: Left: The time and place of origin of every traveling wave produced during a simulation. Right: The FIE clearly shows that traveling waves are likely to start in some regions, and unlikely to start in others.



A separate observation is that only some of the neurons in the SCE will fire when a

wave passes their location. We observe that a single traveling wave initiated by a step stimulus can have regions of higher or lower total firing activity which we quantify by measuring the fractional number of firing events (FFE) per unit length of the SCE. An example measurement of the firing activity in a single traveling wave is shown in Figure 14.

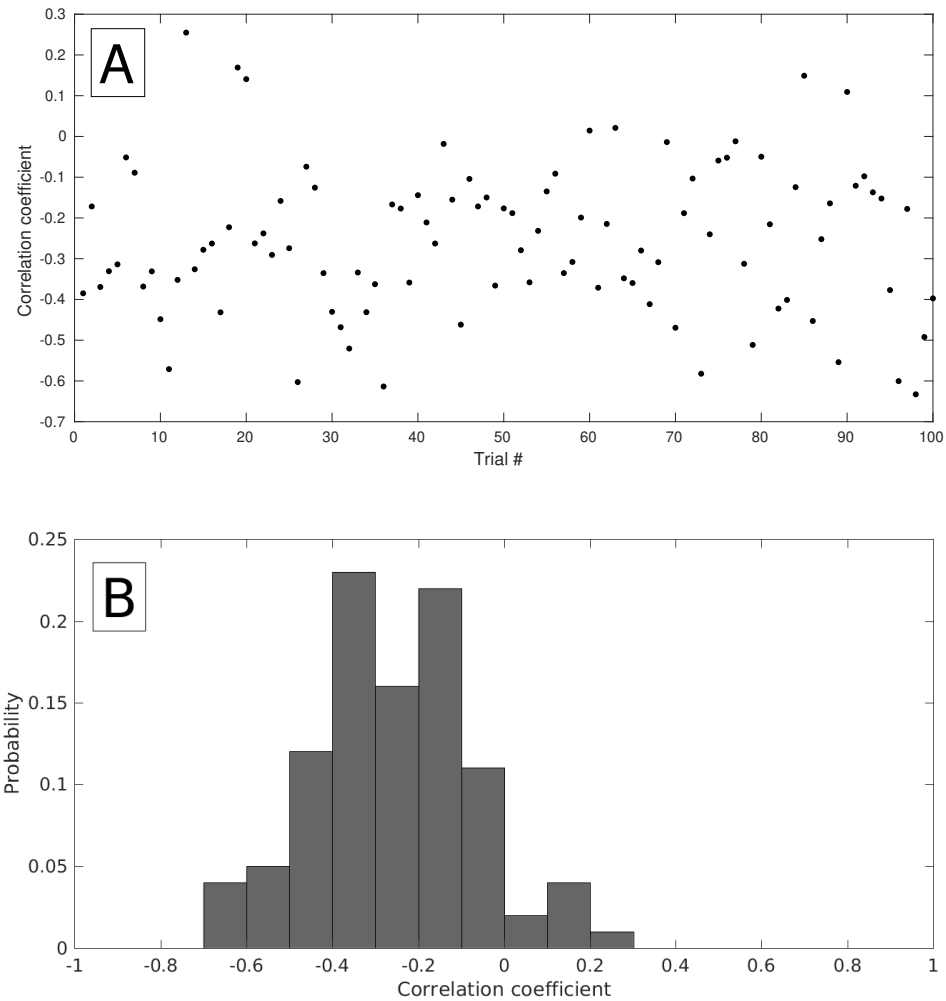
Figure 14: Density of firing events in a traveling wave initiated from a step stimulus. Left: Raster plot of the spike-emission times from a single traveling wave. Right: The FFE shows that some regions of the SCE exhibit more firing activity.



By combining these two experiments we observe that the results from the FIE and the FFE appear anti-correlated for the same SCE (see Figure 3 in Supplemental Information for examples). To test that this observation is generally true we create 100 SCEs, apply first uniform background stimulus and then step stimulus to each SCE, and

measure the correlation between the FIE and FFE (Figure 15). The correlation coefficient is estimated from the two histograms using MATLAB 'corrcoef'. Although there is substantial variation between SCEs we measure a consistently negative correlation coefficient (mean -0.26 , standard deviation 0.18) between FIE and FFE results. A one-sided t-test at the 1% confidence level rejects the null hypothesis that the mean of the correlation coefficient is 0 or greater.

Figure 15: A) Correlation between FIE and FFE across 100 trials. B) Distribution of the correlation coefficient. Each trial is a new SCE with random neuron and connectivity parameters.

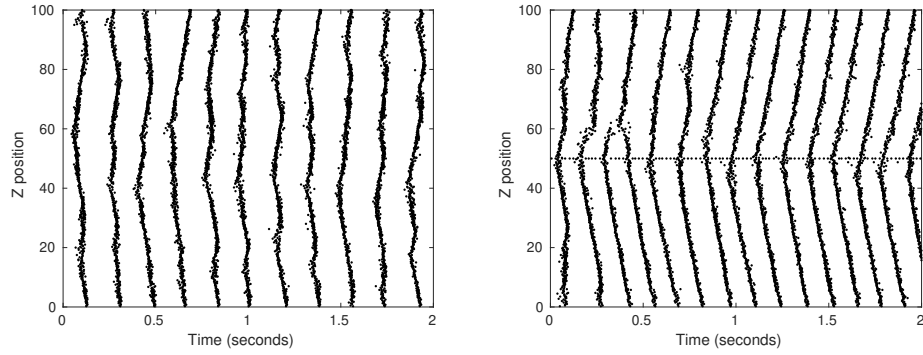


We hypothesize that these preferential wave initiation sites are created by neurons with low firing thresholds that are easy to excite. In the Izhikevich model, inhibitory neurons can have a lower firing threshold than excitatory neurons, modeling the behavior of real inhibitory neurons in the cortex(Gibson et al., 1999)(Hayut, Fanselow, Connors, & Golomb, 2011). As we can see from figure 6 the b parameter in the Izhikevich model sets the firing threshold of the individual neurons. Neurons with higher b parameter are easier to excite and therefore more likely to fire. Per Table 1 excitatory neurons all have a b parameter of 0.2, while inhibitory neurons have b parameters in the range $0.2 - 0.25$. This indicates the preferential wave initiation sites could be due to low-threshold spiking (LTS) inhibitory neurons (Izhikevich, 2003). It may seem counter-intuitive that firing activity from an inhibitory neuron would generate traveling waves. In fact, postinhibitory rebound spiking is observed in both cortical neurons (Ascoli, Gasparini, Medinilla, & Migliore, 2010) and the Izhikevich model of neuron dynamics, and was studied in the context of spindle waves in the thalamus in (Golomb et al., 1996). The LTS hypothesis also explains the reduced wave density at these sites. As a traveling wave passes through the region, because of their increased activity these same inhibitory neurons suppress the surrounding neurons resulting in fewer local firing events.

A comparative computational experiment shows that low-threshold spiking inhibitory neurons can indeed generate traveling waves under background stimulus. We first create an SCE with entirely excitatory neurons. We then create an identical SCE except for a single LTS inhibitory neuron at $Z = 50$. The b parameter of the LTS inhibitory neuron is set to 0.25, corresponding to the lowest firing threshold used in our model.

These two SCEs are stimulated with the same uniform background stimulus. Figure 16 clearly shows that adding the single LTS neuron results in traveling waves emanating from $Z = 50$.

Figure 16: Simulation with a single LTS inhibitory neuron at $Z = 50$. Left: an SCE with entirely excitatory neurons shows traveling waves emerging from various locations. Right: adding a single LTS neuron at $Z = 50$ results in consistent wave generation from that location.



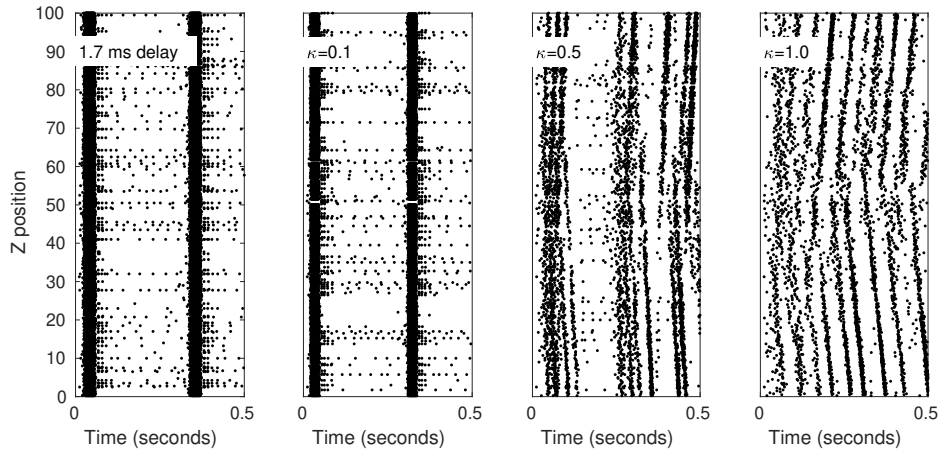
3.4 Wave patterns in fully connected networks

Our investigation has been concerned with traveling waves of activations that spread through locally connected networks. We now examine whether traveling wave patterns can also be observed in fully connected networks. We show that this is possible provided we consider the action potential propagation delay proportional to the distance between neurons, as used in all the simulations above. We simulate an SCE with complete connectivity corresponding to $\lambda \rightarrow \infty$: all neurons are connected with probability 1 to all other neurons. This is analogous to the original Izhikevich simulation (Izhikevich, 2003) that demonstrated synchronized firing in a completely connected neural field with random background stimulus. We first simulate the SCE with a fixed action

potential propagation delay of 1.7 ms (Markram et al., 1997) regardless of inter-neuron distance. The result is highly synchronized simultaneous firing among all neurons in the SCE.

With distance-dependent propagation delays and fast spike propagation ($\kappa = 0.1$) we observe similar synchronized firing. We then increase κ and observe the emergence of traveling wave patterns (Figure 17). This demonstrates that one dimensional traveling waves can emerge from fully-connected networks if the propagation delay is proportional to the inter-neuron distance and the spike propagation time is above a critical value.

Figure 17: With global connectivity and action potential propagation delay fixed at 1.7 ms , the entire structure shows synchronized firing events. With distance-dependent propagation we also observe synchronized firing at $\kappa = 0.1$. As κ increases traveling waves emerge ($\kappa = 0.5, 1.0$) .



The present case is similar to previous work that considered coupled oscillators ((G. Bard Ermentrout & Kleinfeld, 2001), Figure 1) that proposed several models for

traveling waves in the cortex. The one most relevant to traveling waves in our fully-connected networks is a driving source at a spatial location that produces traveling wave patterns due to the propagation delay of action potentials. This is a fundamentally different type of traveling wave than a chain of spike events that spreads to neighboring neurons due to local connectivity.

4 Discussion

Here we have demonstrated that a biologically influenced model of a small quasi one-dimensional columnar ensemble can support traveling waves. Our model considers a wide variety of neuronal types using local connectivity and distance-dependent time delays. Because of the substantial randomness in neuronal types and connections between neurons, we did not observe traveling waves in the purely one-dimensional ($X = 1, Y = 1$) version of our model, in contrast to previous work that considered traveling waves in homogeneous neuronal populations in strictly one-dimensional systems (see SI Figure 6).

In our model various parameters determine traveling wave formation and propagation including the connectivity, connection strength and excitatory/inhibitory balance. Columns with local connectivity support traveling waves, consistent with other simulations and experimental studies of cortical traveling waves (Kopell & Ermentrout, 1986)(G. Bard Ermentrout & Kleinfeld, 2001)(Golomb & Ermentrout, 1999) . The speed of these waves are influenced by connectivity, with a logarithmic dependence on connection strength that is consistent with previous work (Golomb et al., 1996)(Golomb

& Ermentrout, 1999).

We have also shown that a fully-connected SCE exhibits traveling waves if the action potential propagation time depends on the inter-neuron distance. From the dynamics point of view, we have shown that the action potential propagation delays affect propagation speed (Figure 9) but is not a determinant on whether a wave can exist (Figure 4d). We have also shown that the connectivity and connection strengths influence the wave propagation speed (Figures 7 and 11) through the neuron dynamics (Figure 6). From the point of view of neuronal types we have determined that preferential sites for wave initiation are due to the presence of inhibitory neurons with low spiking thresholds.

Previous research into traveling waves in neuronal networks has identified parameter regions of neural-field models for which traveling waves exist (Wilson & Cowan, 1973)(G. B. Ermentrout & Cowan, 1979). In these models critical values of model parameters are usually revealed by a linear stability analysis. Our exploration of model parameters (Figure 4) instead shows a gradual transition region in which waves emerge and dominate the firing activity. In (Senk et al., 2020) the authors derive critical parameters using linear stability analysis of a neural field and find the critical parameter values, then map those parameters to a network of leaky integrate-and-fire neurons. Although the stability analysis shows sharply defined regions (their Figure 3 and 4), their spiking neuron simulation results show a gradual transition between regions (their Figure 7) similar to our work.

We have investigated the effect of incrementally increasing the dimensionality of our SCE on the speed and existence of traveling waves by considering a larger base

(width described by X and Y) but still preserving its quasi one-dimensional character (ratio of Z to X or Y from 50 to greater than 7). Our results show that the speed of the traveling waves initiated at the bottom of the SCE increased as a function of width (Figure 11). This can be understood by noting that we use open boundary conditions that when considering a larger width will inevitably increase the average number of connections per neuron in the SCE. This means that neurons on average will receive a higher input current that, by its similarity to the mechanisms behind Figure 7, will cause a higher speed. We further show that the increased number of connections per neuron is the sole mechanism behind this effect by obtaining a constant speed when keeping constant the average number of connections (Figure 12). By using the same system with a constant number of connections per neuron, but now using a background stimulation to all neurons, we show that the value of the connection strength beyond which traveling waves (or synchronous firing) exist is very similar to that shown in Figure 4a, independent of width of SCE (SI Figure 5). Moreover, the graphs of raster plots as a function of width seem to indicate that there is a value for the width at which excitations change from traveling waves to synchronous firing (SI Figure 5). Future work will consider whether this change represents a phase transition between traveling waves and synchronous firing, a transition that is not uncommon to find in other systems but controlled by other intrinsic coupling parameters (G. Bard Ermentrout & Kleinfeld, 2001)(Senk et al., 2020).

Other research (Keane & Gong, 2015) has shown that complex spatial patterns emerge from two-dimensional networks of leaky-integrate-and-fire neurons when the excitation and inhibition are balanced. In that work, when excitation dominates then

only plane waves were observed instead of complex patterns. Similarly, in one dimension we have found that traveling waves dominate the firing activity when the P_{exc} grows close to 1 (Figure 4). Both studies show that traveling waves can become the dominant spatial pattern in excitatory networks.

We have found that low-threshold-spiking inhibitory neurons can determine the origin point of traveling waves when using a uniform background stimulus (Figure 16). Parameter variations in the Izhikevich model (Izhikevich, 2003) create low-threshold spiking found in some inhibitory neurons (Gibson et al., 1999)(Hayut et al., 2011), leading to post-inhibitory rebound spiking in the connected excitatory neurons (Ascoli et al., 2010). Our result is fundamentally different than previous studies of oscillatory behavior in populations of coupled excitatory and inhibitory neurons (Golomb et al., 1996)(Golomb & Ermentrout, 1999) as that work considered homogeneous populations with isotropic connectivity.

Our result implies that, when no stimulus is applied, a biological neuronal network might have an equilibrium dynamics governed by traveling waves initiated by low-threshold-spiking inhibitory neurons. An applied stimulus could then disturb the network from this dynamic equilibrium state. Our results show that any network with sufficiently strong connectivity and delayed action potential propagation can exhibit traveling wave structure (Figure 17). Since biological action potentials always travel with some delay, this indicates that traveling waves could be observed in the brain regardless of the inter-neuron connectivity. The numerical results presented here could be further refined to predict biological traveling wave speed for different neuron and network parameters. This could help distinguish between the different classes of traveling

waves presented in (G. Bard Ermentrout & Kleinfeld, 2001).

Traveling waves in one-dimensional networks have not been observed in the brain. Part of the reason might be that such an observation requires precise experiments that probe structures such as minicolumns in the cortex. These are not easy, as other properties of minicolumns are still elusive. However, our work shows that in biological quasi one-dimensional systems traveling waves are not only possible, but that because of the wide range of values in their allowed parameter space, their existence should be expected.

References

- Ascoli, G. A., Gasparini, S., Medinilla, V., & Migliore, M. (2010). Local control of postinhibitory rebound spiking in CA1 pyramidal neuron dendrites. *Journal of Neuroscience*, 30(18), 6434–6442. doi:10.1523/JNEUROSCI.4066-09.2010
- Atay, F. M. & Hutt, A. (2006, December). Neural fields with distributed transmission speeds and long-range feedback delays. *SIAM Journal on Applied Dynamical Systems*, 5(4), 670–698. doi:10.1137/050629367
- Bressloff, P. C. & Coombes, S. (1997). Synchrony in an Array of Integrate-and-Fire Neurons with Dendritic Structure. *Physical Review Letters*, 78(24), 4665–4668. doi:10.1103/PhysRevLett.78.4665
- Buxhoeveden, D. P. & Casanova, M. F. (2002). The minicolumn hypothesis in neuroscience. *Brain*, 125(5), 935–951. doi:10.1093/brain/awf110
- Chervin, R. D., Pierce, P. A., & Connors, B. W. (1988). Periodicity and directionality in the propagation of epileptiform discharges across neocortex. *Journal of Neurophysiology*, 60(5), 1695–1713. doi:10.1152/jn.1988.60.5.1695
- Cruz, L., Roe, D. L., Urbanc, B., Inglis, A., Stanley, H. E., & Rosene, D. L. (2009). Age-related reduction in microcolumnar structure correlates with cognitive decline in ventral but not dorsal area 46 of the rhesus monkey. *Neuroscience*, 158(4), 1509–1520. doi:10.1016/j.neuroscience.2008.11.033
- Ermentrout, G. B. [G. B.] & Cowan, J. D. (1979). Temporal oscillations in neuronal nets. *Journal of Mathematical Biology*, 7(3), 265–280. doi:10.1007/BF00275728

- Ermentrout, G. B. [G. Bard] & Kleinfeld, D. (2001). Traveling electrical waves in cortex: Insights from phase dynamics and speculation on a computational role. *Neuron*, 29(1), 33–44. doi:10.1016/S0896-6273(01)00178-7
- Ferezou, I., Bolea, S., & Petersen, C. C. (2006, May). Visualizing the Cortical Representation of Whisker Touch: Voltage-Sensitive Dye Imaging in Freely Moving Mice. *Neuron*, 50(4), 617–629. doi:10.1016/j.neuron.2006.03.043
- Fino, E. & Yuste, R. (2011). Dense inhibitory connectivity in neocortex. *Neuron*, 69(6), 1188–1203. doi:10.1016/j.neuron.2011.02.025
- Folias, S. E. & Ermentrout, G. B. [G. Bard]. (2012, August). Bifurcations of stationary solutions in an interacting pair of E-I neural fields. *SIAM Journal on Applied Dynamical Systems*, 11(3), 895–938. doi:10.1137/110860094
- Gibson, J. R., Belerlein, M., & Connors, B. W. (1999). Two networks of electrically coupled inhibitory neurons in neocortex. *Nature*, 402(6757), 75–79. doi:10.1038/47035
- Golomb, D. & Amitai, Y. (1997). Propagating neuronal discharges in neocortical slices: Computational and experimental study. *Journal of Neurophysiology*, 78(3), 1199–1211. doi:10.1152/jn.1997.78.3.1199
- Golomb, D. & Ermentrout, G. B. [G. Bard]. (1999). Continuous and lurching traveling pulses in neuronal networks with delay and spatially decaying connectivity. *Proceedings of the National Academy of Sciences of the United States of America*, 96(23), 13480–13485. doi:10.1073/pnas.96.23.13480

- Golomb, D., Wang, X. J., & Rinzel, J. (1996). Propagation of spindle waves in a thalamic slice model. *Journal of Neurophysiology*, 75(2), 750–769. doi:10.1152/jn.1996.75.2.750
- Hayut, I., Fanselow, E. E., Connors, B. W., & Golomb, D. (2011). LTS and FS inhibitory interneurons, short-term synaptic plasticity, and cortical circuit dynamics. *PLoS Computational Biology*, 7(10). doi:10.1371/journal.pcbi.1002248
- Horton, J. G. & Adams, D. L. (2005). The cortical column: A structure without a function. *Philosophical Transactions of the Royal Society B: Biological Sciences*, 360(1456), 837–862. doi:10.1098/rstb.2005.1623
- Huang, X., Troy, W. C., Yang, Q., Ma, H., Laing, C. R., Schiff, S. J., & Wu, J. Y. (2004). Spiral waves in disinhibited mammalian neocortex. *Journal of Neuroscience*, 24(44), 9897–9902. doi:10.1523/JNEUROSCI.2705-04.2004
- Izhikevich, E. M. (2003). Simple model of spiking neurons. *IEEE Transactions on Neural Networks*, 14(6), 1569–1572. doi:10.1109/TNN.2003.820440
- Keane, A. & Gong, P. (2015). Propagating waves can explain irregular neural dynamics. *Journal of Neuroscience*, 35(4), 1591–1605. doi:10.1523/JNEUROSCI.1669-14.2015
- Kopell, N. & Ermentrout, G. B. [G. B.]. (1986, September). Symmetry and phaselocking in chains of weakly coupled oscillators. *Communications on Pure and Applied Mathematics*, 39(5), 623–660. doi:10.1002/cpa.3160390504
- Levy, R. B. & Reyes, A. D. (2012). Spatial profile of excitatory and inhibitory synaptic connectivity in mouse primary auditory cortex. *Journal of Neuroscience*, 32(16), 5609–5619. doi:10.1523/jneurosci.5158-11.2012

- Lubenov, E. V. & Siapas, A. G. (2009). Hippocampal theta oscillations are travelling waves. *Nature*, 459(7246), 534–539. doi:10.1038/nature08010
- Maass, W., Natschläger, T., & Markram, H. (2002). Real-time computing without stable states: A new framework for neural computation based on perturbations. *Neural Computation*, 14(11), 2531–2560. doi:10.1162/089976602760407955
- Markram, H., Lübke, J., Frotscher, M., Roth, A., & Sakmann, B. (1997, April). Physiology and anatomy of synaptic connections between thick tufted pyramidal neurones in the developing rat neocortex. *Journal of Physiology*, 500(2), 409–440. doi:10.1113/jphysiol.1997.sp022031
- Mountcastle, V. B. (1997). The columnar organization of the neocortex. *Brain*, 120(4), 701–722. doi:10.1093/brain/120.4.701
- Muller, L., Chavane, F., Reynolds, J., & Sejnowski, T. J. (2018). Cortical travelling waves: Mechanisms and computational principles. *Nature Reviews Neuroscience*, 19(5), 255–268. doi:10.1038/nrn.2018.20
- Muller, L., Reynaud, A., Chavane, F., & Destexhe, A. (2014). The stimulus-evoked population response in visual cortex of awake monkey is a propagating wave. *Nature Communications*, 5. doi:10.1038/ncomms4675
- Pyle, R. & Rosenbaum, R. (2017). Spatiotemporal Dynamics and Reliable Computations in Recurrent Spiking Neural Networks. *Physical Review Letters*, 118(1), 1–5. doi:10.1103/PhysRevLett.118.018103. arXiv: 1611.01557
- Qi, Y. & Gong, P. (2015). Dynamic patterns in a two-dimensional neural field with refractoriness. *Physical Review E - Statistical, Nonlinear, and Soft Matter Physics*, 92(2), 1–13. doi:10.1103/PhysRevE.92.022702

Reimer, A., Hubka, P., Engel, A. K., & Kral, A. (2011). Fast propagating waves within the rodent auditory cortex. *Cerebral Cortex*, 21(1), 166–177. doi:10.1093/cercor/bhq073

Riehle, A., Wirssohn, S., Grün, S., & Brochier, T. (2013, March). Mapping the spatio-temporal structure of motor cortical LFP and spiking activities during reach-to-grasp movements. *Frontiers in Neural Circuits*, 7(MAR), 48. doi:10.3389/fncir.2013.00048

Roxin, A., Brunel, N., & Hansel, D. (2005). Role of delays in shaping spatiotemporal dynamics of neuronal activity in large networks. *Physical Review Letters*, 94(23), 1–4. doi:10.1103/PhysRevLett.94.238103

Rubino, D., Robbins, K. A., & Hatsopoulos, N. G. (2006). Propagating waves mediate information transfer in the motor cortex. *Nature Neuroscience*, 9(12), 1549–1557. doi:10.1038/nn1802

Sanes, J. N. & Donoghue, J. P. (1993). Oscillations in local field potentials of the primate motor cortex during voluntary movement. *Proceedings of the National Academy of Sciences of the United States of America*, 90(10), 4470–4474. doi:10.1073/pnas.90.10.4470

Sato, T. K., Nauhaus, I., & Carandini, M. (2012). Traveling Waves in Visual Cortex. *Neuron*, 75(2), 218–229. doi:10.1016/j.neuron.2012.06.029

Senk, J., Korvasová, K., Schuecker, J., Hagen, E., Tetzlaff, T., Diesmann, M., & Helias, M. (2020, May). Conditions for wave trains in spiking neural networks. *Phys. Rev. Research*, 2(2), 23174. doi:10.1103/PhysRevResearch.2.023174

- Shoham, D., Glaser, D. E., Arieli, A., Kenet, T., Wijnbergen, C., Toledo, Y., ... Grinvald, A. (1999). Imaging cortical dynamics at high spatial and temporal resolution with novel blue voltage-sensitive dyes. *Neuron*, 24(4), 791–802. doi:10.1016/S0896-6273(00)81027-2
- Strogatz, S. H. & Mirollo, R. E. (1991, May). Stability of incoherence in a population of coupled oscillators. *Journal of Statistical Physics*, 63(3-4), 613–635. doi:10.1007/BF01029202
- Townsend, R. G. & Gong, P. (2018). Detection and analysis of spatiotemporal patterns in brain activity. *PLoS Computational Biology*, 14(12), 1–29. doi:10.1371/journal.pcbi.1006643
- Williams, T. L. & Bowtell, G. (1997). The calculation of frequency-shift functions for chains of coupled oscillators, with application to a network model of the lamprey locomotor pattern generator. *Journal of Computational Neuroscience*, 4(1), 47–55. doi:10.1023/A:1008864410375
- Wilson, H. R. & Cowan, J. D. (1973). A mathematical theory of the functional dynamics of cortical and thalamic nervous tissue. *Kybernetik*, 13(2), 55–80. doi:10.1007/BF00288786
- Wu, J. Y., Huang, X., & Zhang, C. (2008). Propagating waves of activity in the neocortex: What they are, what they do. *Neuroscientist*, 14(5), 487–502. doi:10.1177/1073858408317066
- Wyller, J., Blomquist, P., & Einevoll, G. T. (2007, January). Turing instability and pattern formation in a two-population neuronal network model. *Physica D: Nonlinear Phenomena*, 225(1), 75–93. doi:10.1016/j.physd.2006.10.004

Xu, W., Huang, X., Takagaki, K., & young Wu, J. (2007). Compression and Reflection of Visually Evoked Cortical Waves. *Neuron*, 55(1), 119–129. doi:10.1016/j.neuron.2007.06.016